A 2D GaAs-Based Photonic Crystal Biosensor for Malaria Detection

Manjunatha N[1], Sarika Raga[1,*], Sanjay Kumar Gowre[2], Hameed Miyan[3]

[1]Department of Electronics and Communication Engineering, Visvesvaraya Technological University, Centre for Post Graduate Studies, Muddenahalli, Chikkaballapur, India

[2]Department of Electronics and Telecommunication Engineering, School of Electrical and Communication Sciences, JSPM University, Pune, India

[3]Department of Electronics and Communication Engineering, Bheemanna Khandre Institute of Technology, Bhalki, Bidar, India

Received 02 March 2023; received in revised form 27 April 2023; accepted 07 June 2023

DOI: https://doi.org/10.46604/ijeti.2023.11660

Abstract

Gallium arsenide (GaAs) composite semi-conductive rods with an air background lattice act as the building blocks for the photonic crystal structure used of a biosensor. The study presents a biosensor of a two-rod nano-cavity for identifying distinct stages of plasmodium falciparum in red blood cells (RBCs) in the early detection of malaria. The proposed biosensor enables the creation of a label-free biosensing environment in which optical and dispersion properties are investigated using plane wave expansion (PWE) and finite-difference time-domain (FDTD) techniques. The biosensor, with a sensing region for an analyte, is utilized to detect a change in refractive index to differentiate between normal RBCs and plasmodium falciparum-infected cells. The results show that the biosensor has a high sensitivity of 798.143 nm/RIU, a high Q-factor of 9881.926, a low detection limit (δ) of 222.4×10^{-6} RIU, a high FOM of 4496.079 RIU^{-1}, and a compact area of 46.14 μm^2.

Keywords: photonic crystal, biosensor, plasmodium falciparum, sensitivity, quality factor

1. Introduction

Malaria is the most prevalent tropical and subtropical illness caused by a parasite transmitted through female anopheles mosquito bites. Plasmodium (P) falciparum, P. knowlesi, P. ovale, P. malariae, and P. vivax are the five subtypes of the malaria disease. The most deadly form of malaria is P. falciparum [1-2]. Malaria infection damages red blood cells (RBCs), affects the liver and kidneys, and inhibits breathing. The World Health Organization estimated 241 million cases and 0.627 million deaths in 2020. Malaria-infected RBCs have three stages: the early ring stage (R-stage, 0 to 8 hours), the trophozoite stage (T-stage, 8 to 24 hours), and the schizont stage (S-stage, 24 to 40 hours). The refractive index (RI) is measured using tomographic phase microscopy (TPM) and diffraction phase microscopy (DPM) to collect data at each stage, generating three-dimensional maps of RI and nanoscale cell membrane variations in isolated RBCs [3].

Traditional methods for malaria detection include microscopy [4], rapid diagnostic tests (RDTs) [5], polymerase chain reaction (PCR) [6], loop-mediated isothermal amplification (LAMP) [7], saliva-based tests for nucleic-acid amplification [8], saliva-based test for plasmodium protein detection [9], transdermal hemozoin detection [10], and urine malaria test (UMT) [11]. These technologies require significant investment, well-trained technicians, and specialized laboratory facilities. Photonic crystal (PC)-based sensors have been developed to fulfill the requirements of high sensitivity, reliability, quick response, high accuracy, and real-time detection. PC is a periodic dielectric structure with a photonic band gap (PBG), typically consisting of

* Corresponding author. E-mail address: raga.sarika@vtu.ac.in

English language proofreader: Chih-Wen Teng

cylindrical dielectric rods in an air slab or an air hole in a dielectric slab. By introducing point, line, or combination defects in PCs, light inside PBG can be localized [12]. Light propagation in PC PBG features is described by Maxwell's equations. PC-based sensors have found numerous applications, including temperature sensing [13], pressure sensing [14], gas sensing [15], mechanical sensing [16], biosensing [17-18], and many more in the past decade.

In recent years, there have been significant improvements in the performance parameters of biosensors, including sensitivity, quality factor (Q-factor), figure of merit (FOM), and detection limit (δ). One such improvement is the use of a 20 × 24-PC lattice structure with a SiO_2 substrate and Si slab containing air holes. The design incorporates Z-shaped waveguides with a tuning factor point defect and ring neighboring holes that are adjusted in small steps to maximize the Q-factor. The resulting biosensor exhibits a Q-factor of 214, a sensitivity of 225 nm/RIU, a FOM of 22.5 RIU^{-1}, a δ of 0.044 RIU, and an area of 100 μm^2 [19].

Another design involves a 13 × 21-PC square lattice composed of elliptical gold rods with an air background. Two linear waveguides and a ring resonator utilize a silicon nitride (Si_3N_4) rod to carry input and output waves. The first biosensor in this design achieves a Q-factor of 152.543 and a sensitivity of 356.915 nm/RIU. The second design features a Q-factor of 212.771, a sensitivity of 898.9764 nm/RIU, and an area of 58.92 μm^2 [20]. Similarly, a 23 × 39-PC hexagonal lattice structure consisting of a Si slab with air holes, along with two linear waveguides and one point defect, is developed. This biosensor demonstrates a Q-factor of 9825.3, a sensitivity of 325.13 nm/RIU, a FOM of 14771.048 RIU^{-1}, a δ of 6.77×10^{-5} RIU, and an area of 143.52 μm^2 [21].

Additionally, a 23 × 24-PC lattice structure with a Si slab and air holes is designed, incorporating two-point defects and a hexagonal cavity with a varying cavity radius. The first biosensor achieves a Q-factor of 2576.14, a sensitivity of 161.42 nm/RIU, and an area of 104.88 μm^2. The second design features a Q-factor of 5978.36, a sensitivity of 137 nm/RIU, and an area of 51.7 μm^2 [22]. Furthermore, a 1D-PC design is implemented using Si and fused Si defect layers. This biosensor demonstrates a Q-factor of 2.03×10^5, a sensitivity of 495.73 nm/RIU, a FOM of 1.239×10^5 RIU^{-1}, and a δ of 8.07×10^{-5} RIU [23]. Another 1D-PC design utilizes N layers of Si and lanthanum flint on each side, with a defect layer in the middle to analyze changes in defect layer thickness. This design achieves a Q-factor of 6.938947×10^4, a sensitivity of 327.7 nm/RIU, and a FOM of 3.277×10^4 RIU^{-1} [24]. As mentioned earlier, it is crucial to improve biosensor sensitivity and Q-factor, along with other parameters such as the FOM and δ.

This paper proposes a biosensor of a two-rod nano-cavity that acts as a sensing region, surrounded by gallium arsenide (GaAs) rods with air in the background, and two linear waveguides. The biosensor replaces the RI of the target sample, which changes from normal RBC (N-stage) to infected RBC with malaria stages, and each stage is tested separately. A shift in the resonant wavelength to different values is detected at the output of the waveguide [25]. The proposed work is analyzed using finite-difference time-domain (FDTD) with an anisotropic perfectly matched layer (APML) absorbing boundary [26].

2. Proposed Design

The design of the proposed bio-sensing platform utilizes a 2D-PC structure shown in Fig. 1(a). GaAs rods with RI = 3.374 are arranged in a hexagonal pattern on an air background with RI = 1. The use of a low RI air background in conjunction with high GaAs dielectric rods helps minimize material dispersion and absorption issues. The initial distance between two adjacent rods is considered as the lattice constant, assumed to be a = 1000 nm, while the radii of GaAs rods are set to r = 0.2 a (200 nm). The dimension of the 2D structure is 11 × 13 μm^2. The operating wavelength of the input source is 1550 nm, chosen as the optimal wavelength for biosensing [27-28]. The plane wave expansion (PWE) technique is used to compute the dispersion diagram of PBG for a normalized frequency range of $0.282 < a/\lambda < 0.452$, resulting in the transverse electric (TE) mode as shown in Fig. 1(b). To calculate the necessary lattice constant, a bandgap value slightly below $a/\lambda = 0.452$ is considered, and

a/λ = 0.4065 is chosen. With λ = 1550 nm, the calculated lattice constant is a = 630 nm, (and the rod radius is) r = 0.2 a = 126 nm. The range of gap wavelength corresponds to 1394 nm to 2234 nm, which meets the sensing requirements. Based on this updated lattice constant, the biosensor occupies a compact area of 46.14 μm^2. Fig. 1 illustrates the 2D-PC lattice structure and the TE mode photonic band structure. All simulation results are obtained using the OptiFDTD simulation software.

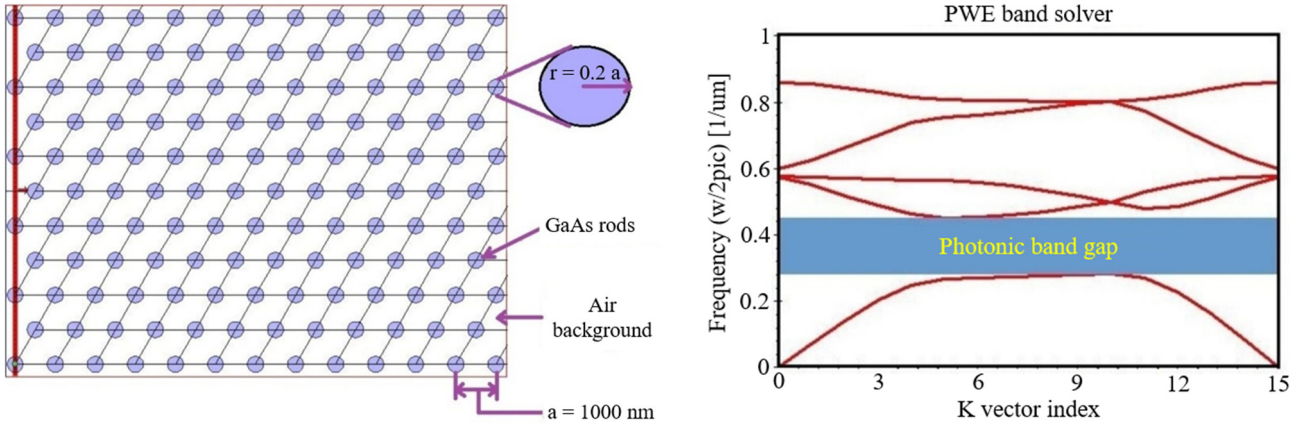

(a) 2D hexagonal PC structure (a = 1000 nm, r = 200 nm) (b) TE mode band structure (a = 1000 nm, r = 0.2 a)

Fig. 1 2D-PC structure and TE mode band-structure

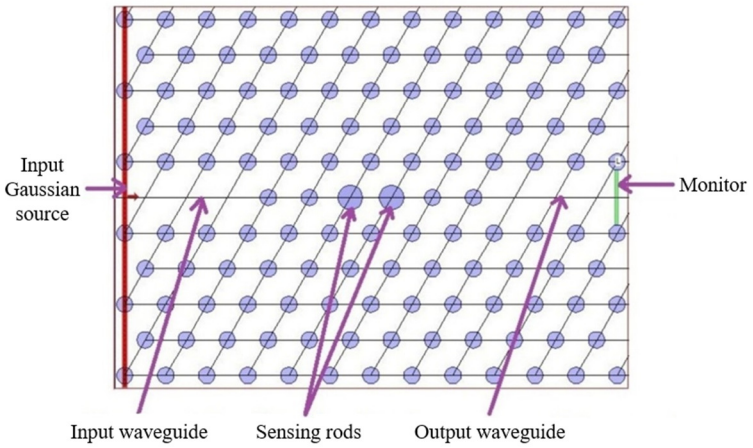

(a) 2D-PC-based biosensor with point defects

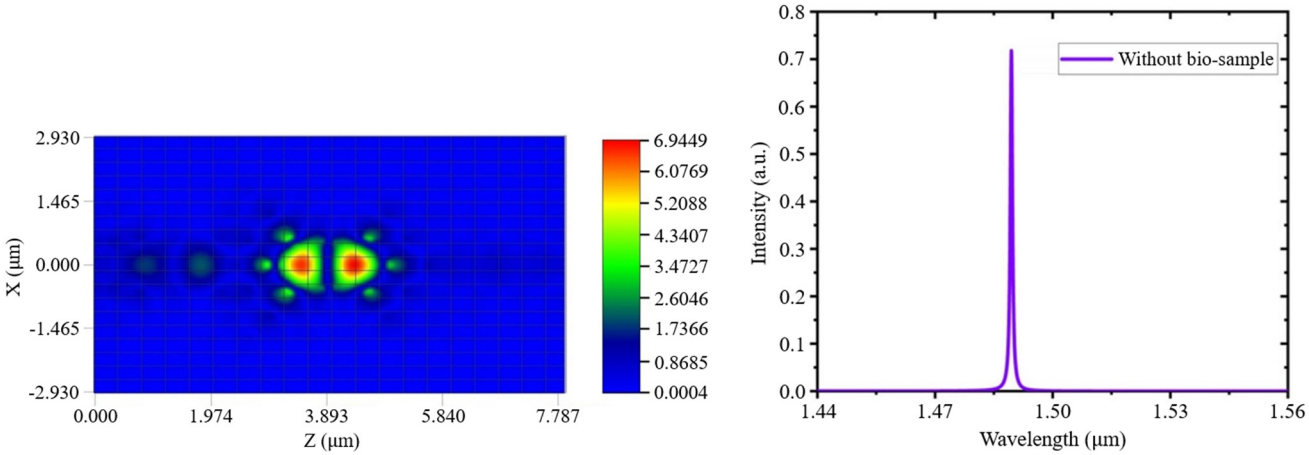

(b) Normalized electric field intensity (c) Sensing region transmission spectrum without bio-sample (air reference)

Fig. 2 2D-PC structure, normalized electric field intensity plot, and transmission spectra

After designing the 2D-PC with the desired wavelength bandgap, a point defect is induced to disrupt the periodic nature of the PC. This can be achieved by eliminating GaAs rods, modifying their material properties, or altering their sizes. Consequently, this results in a guided mode within the band gap region. In this instance, all types of defects were considered

to achieve the optimal performance of the sensor. Using point defects of the two center rods coupled with the input and output waveguides, the sensing region is formed. By removing the GaAs rods, the waveguides were created as shown in Fig. 2(a). An optical source light is launched at the input waveguide and a monitor is located at the output waveguide. For a guided optical mode with no analyte within the sensing region, light is completely localized within the sensing region of the PC and acts as a resonator, as shown in Fig. 2(b). The resonance wavelength measured at the monitor is 1489 nm as shown in Fig. 2(c). Fig. 2 shows the design, electric field intensity, and transmission spectrum of the 2D-PC biosensor.

To observe a resonant shift of the designed sensor, blood samples ranging from N-stages to various stages of malaria were evaluated.

$$\in = \eta^2 \tag{1}$$

According to Eq. (1), the permittivity ($\in$) of the various blood samples differs. A small change in RI (η) and corresponding $\in$ gets changed by η square.

In the initial phase of malaria, the patient's hemoglobin level is marginally lower than normal. As time passes, the level of hemoglobin decreases, resulting in a decrease in the RI of the blood cells. Table 1 shows the RI values for normal and various stages of malaria disease.

Table 1 Refractive index (RI) of malaria disease at different stages [3]

Different stages of malaria disease	Hemoglobin content (g/dL)	Refractive index (η)
Normal RBC (N-stage)	28-36	1.402
Ring stage (R-stage)	24-29	1.395
Trophozoite stage (T-stage)	19.78-22.88	1.383
Schizont stage (S-stage)	16.28-19.38	1.373

The performance of a sensor is characterized by various parameters, including sensitivity, Q-factor, δ, and FOM [29]. The sensitivity is measured as the ratio of the change in resonant wavelength to the change in the used bio-samples RI.

$$\text{Sensitivity} = \Delta\lambda_0/\Delta\eta \tag{2}$$

where $\Delta\lambda_0 = |\Delta\lambda_{02} - \Delta\lambda_1|$ is the wavelength shift between normal and malaria-infected disease, and $\Delta\eta = |\eta_{02} - \eta_1|$ is the corresponding change in RI. The Q-factor of an optical cavity quantifies the cavity's electromagnetic energy storage capacity.

$$\text{Q-factor} = \lambda_0/\text{FWHM} \tag{3}$$

where $\text{FWHM} = |\lambda_2 - \lambda_1|$ is the full width at half maximum (FWHM), which is obtained by taking into account the wavelength difference at 50 % of the peak amplitude. In the presence of optical losses, sensor optimization is guided by the δ.

$$\delta = \text{FWHM}/\text{S} \tag{4}$$

A sensor's FOM is its precision.

$$\text{FOM} = \text{S}/\text{FWHM} = 1/\delta \tag{5}$$

3. Analysis for the Detection of Malaria Disease

As a result of FDTD simulations, it is assumed that the RI of the sensing rods in PC is affected by the different stages of RBCs listed in Table 1. Experimental observations show variations in the output transmission spectra for three distinct stages of malaria disease and N-stages. Fig. 3 shows the transmission spectra of N-stages and infected malaria stages. When the sensing region is induced in someone in good health with N-stages, the resonant wavelength is measured at 1762.167 nm. If

N-stages are replaced by RBCs in an early R-stage of malaria, characterized by an RI = 1.395, the resonant wavelength shifts to 1756.58 nm. It is observed that as the RI decreases, the wavelength also decreases. This is because the transmission velocity of light increases as it passes through an analyte with a lower RI. Fig. 3(a) shows a wavelength shift of 5.587 nm between N-stage and R-stage RBCs. The performance parameters of the proposed sensor are calculated using Eqs. (2)-(5), resulting in a sensitivity = 798.143 nm/RIU, a Q-factor = 8404.688, a $\delta = 261.8 \times 10^{-6}$ RIU, and a FOM = 3818.861 RIU^{-1}.

The resonant shift spectrum between N-stages and the T-stage of malaria disease is shown in Fig. 3(b). Observations indicate that the T-stage resonant wavelength is practically 1747.1 nm, with a shift of 15.067 nm due to a change in RI of 0.019, leading to a sensitivity = 793 nm/RIU, a Q-factor = 9393.01, a $\delta = 234.5 \times 10^{-6}$ RIU, and a FOM = 4263.44 RIU^{-1}. In contrast, the red spectrum shifts by practically 22.948 nm when N-stages are replaced with the S-stage of malaria disease, which has a resonant wavelength of 1739.219 nm, as shown in Fig. 3(c). For this instance, a sensitivity = 791.31 nm/RIU, a Q-factor = 9881.926, a $\delta = 222.4 \times 10^{-6}$ RIU, and a FOM = 4496.079 RIU^{-1} were determined.

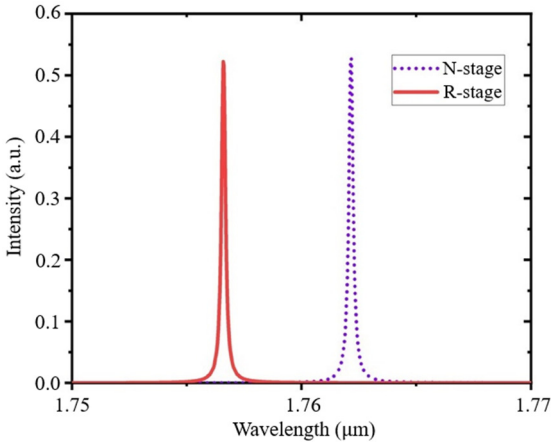

(a) Transmission spectra for N-stage and R-stage

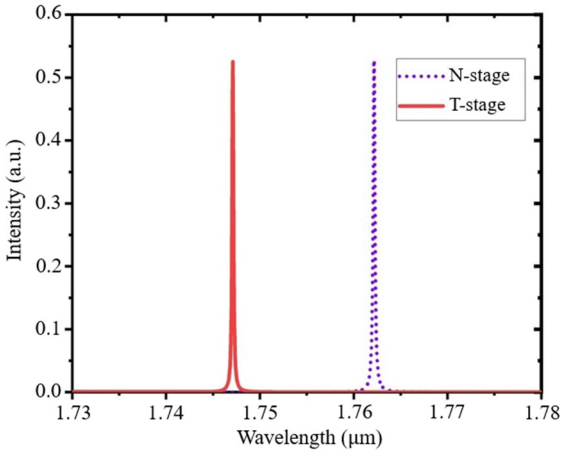

(b) Transmission spectra for N-stage and T-stage

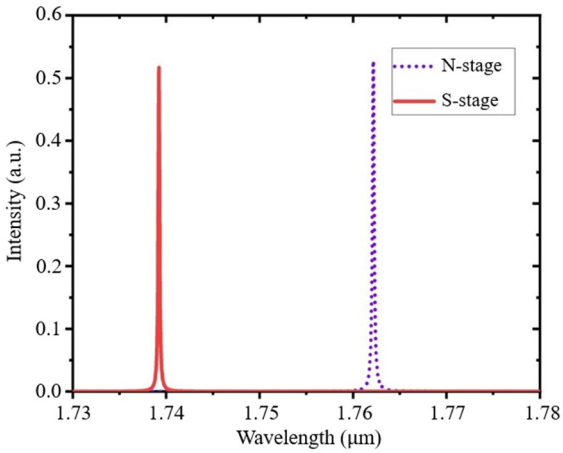

(c) Transmission spectra for N-stage and S-stage

Fig. 3 Transmission spectra for normal (N) stage and malaria-infected (R, T, and S) stages

According to the previous discussion, the proposed structure achieved the highest sensitivity of approximately 798.143 nm/RIU for the R-stage of malaria. It indicates that a significant amount of light interacts with the R-stage blood cells in the proposed structure. Additionally, a Q-factor value of practically 9881.926 was attained for S-stage malaria, indicating a longer lifetime of photons in the sensing cavity compared to other stages of malaria blood cells.

To evaluate the optimized performance of the proposed device, the geometric parameters of the cavity's two central rods were varied. The sensing rod's radius (r_c) of the inside rod in the sensing cavity was optimized by varying it from 0.18 a to 0.48 a in increments of 0.1 a, where a = 630 nm keeps all other parameters constant. The primary objective of this optimization was to achieve a distinct red spectrum shift in the resonant wavelength with a small change in RI in the sensing region, as well

as to improve sensitivity and Q-factor. Generally, sensitivity and Q-factor exhibit opposing tendencies; consequently, it is necessary to optimize the structure to ensure both parameters remain optimal. The results of the optimization are illustrated in Table 2.

Table 2 Sensor parameters with sensing rods radius (r_c) vary from 0.18 a to 0.48 a and a = 0.630 µm, other rods radius (r)

Bio-sample	Sensor parameters	r = 0.2 a = 0.126 µm			
		r_c = 0.18 a (0.1134 µm)	r_c = 0.28 a (0.1764 µm)	r_c = 0.38 a (0.2394 µm)	r_c = 0.48 a (0.3024 µm)
Ring stage (R-stage, η = 1.395; $\Delta\eta$ = 0.007)	$\Delta\lambda_0$ (nm)	1.487	3.189	4.579	5.587
	FWHM (nm)	0.418	0.559	0.197	0.209
	Sensitivity (nm/RIU)	212.428	455.571	654.142	798.143
	Q-factor	3706.985	2896.300	8579.258	8404.688
	FOM (RIU^{-1})	508.202	814.975	3320.517	3818.861
	δ (RIU)	0.00196	0.001227	0.0003011	0.0002618
Trophozoite stage (T-stage, η = 1.383; $\Delta\eta$ = 0.019)	$\Delta\lambda_0$ (nm)	3.966	8.54	12.322	15.067
	FWHM (nm)	0.403	0.569	0.233	0.186
	Sensitivity (nm/RIU)	208.736	449.474	648.526	793
	Q-factor	3838.811	2835.994	7220.476	9393.010
	FOM (RIU^{-1})	517.957	789.936	2783.373	4263.440
	δ (RIU)	0.00193	0.001266	0.000359	0.0002345
Schizont stage (S-stage, η = 1.373; $\Delta\eta$ = 0.029)	$\Delta\lambda_0$ (nm)	5.996	12.961	18.722	22.948
	FWHM (nm)	0.395	0.558	0.252	0.176
	Sensitivity (nm/RIU)	206.758	446.931	645.586	791.310
	Q-factor	3911.420	2883.978	6650.678	9881.926
	FOM (RIU^{-1})	523.439	800.952	2561.849	4496.079
	δ (RIU)	0.00191	0.001248	0.000390	0.0002224

In Table 2, the R-stage of malaria has the highest sensitivity of 798.143 nm/RIU and a Q-factor of 8404.688, while the S-stage shows a sensitivity of 791.310 nm/RIU and the highest Q-factor of 9881.926. When comparing the S-stage, the sensitivity decreased by 6.833 nm/RIU, but there is a significant increase in the Q-factor by 1477.238. As the radius of the sensing region increases, it is capable of accommodating a larger amount of target samples, resulting in increased light-matter interaction and an increase in sensitivity. Nevertheless, the photon lifetime decreases in the cavity, resulting in a slight decrease in the Q-factor, and as the radius of the sensing rods increases, the size of the sensing region increases proportionally.

Table 3 shows the comparison between the proposed design and the previously reported PC structures. It describes the biosensor's structure, materials, sensitivity, Q-factor, FOM, δ, and surface area. This demonstrates that the proposed design is sensitive and has a high Q-factor. In addition, a biosensor has a much smaller surface area than previously reported designs. This biosensor is an ideal candidate for the future detection of malaria disease kits.

Table 3 Comparison of previously reported vs. proposed PC biosensor parameters

Biosensor structure	Materials		Sensitivity (nm/RIU)	Q-factor	FOM (RIU^{-1})	δ (RIU)	Area (μm^2)	Ref.
Z-shaped waveguide with single-point defect	SiO_2 substrate, Si slab with air holes		225	214	22.5	4.4×10^{-2}	100	[19]
Two linear waveguides and ring resonator	Gold rods with air background and Si_3N_4 rods on waveguides	Design 1	356.915	152.513	-	-	58.92	[20]
		Design 2	898.976	212.771				
Two linear waveguides and single-point defect	Si slab with air holes		325.13	9825.3	14.77×10^3	67.7×10^{-6}	143.52	[21]

Table 3 Comparison of previously reported vs. proposed PC biosensor parameters (continued)

Biosensor structure	Materials		Sensitivity (nm/RIU)	Q-factor	FOM (RIU^{-1})	δ (RIU)	Area (μm^2)	Ref.
Two linear waveguides and point defect	Si rods with an air background	Design 1	161.42	2576.14	-	-	104.88	[22]
		Design 2	137	7187.27			51.7	
1-D with a defect layer in the structure	Si and fused Si material		495.73	2.03×10^5	123.91×10^3	8.07×10^{-6}	-	[23]
1-D with a defect layer, without coated walls in the structure	Si and lanthanum flint material		327.7	6.938947×10^4	3.277×10^4	-	-	[24]
Two linear waveguides and two-point defects	GaAs rods with an air background		798.143	9881.926	4496.079	222.4×10^{-6}	46.14	Proposed work

4. Conclusions

The proposed PC-based biosensor structure incorporates point and line defects in a GaAs rod on an air background. It utilizes two-rod nano-cavity as sensing regions to detect each stage of malaria disease. The RI wavelength shift sensing technique, combined with the FDTD method, enables the analysis of different stages of malaria cells. The biosensor demonstrates sharp resonance in the transmission waveform, allowing for differentiation between distinct stages of malaria detection. Through the optimization of the biosensor's performance, including the variation of the sensing region's radius, it achieves a high sensitivity of 798.143 nm/RIU, a high Q-factor of 9881.926, a high FOM of 4496.079 RIU^{-1}, and a low δ of 222.4×10^{-6} RIU. The reported structure is simple to fabricate and occupies a smaller area of 46.14 μm^2, making it well-suited for label-free bio-sensing in biomedical applications such as early malaria diagnosis.

Acknowledgment

This work is supported by the All India Council for Technical Education (AICTE) for financial assistance as JRF/SRF to Manjunatha N (S202173) under the AICTE Doctoral Fellowship (ADF) scheme.

Conflicts of Interest

The authors declare no conflict of interest.

References

[1] J. Molina-Franky, L. Cuy-Chaparro, A. Camargo, C. Reyes, M. Gómez, D. R. Salamanca, et al., "Plasmodium Falciparum Pre-Erythrocytic Stage Vaccine Development," Malaria Journal, vol. 19, article no. 56, 2020.

[2] K. V. Ragavan, S. Kumar, S. Swaraj, and S. Neethirajan, "Advances in Biosensors and Optical Assays for Diagnosis and Detection of Malaria," Biosensors and Bioelectronics, vol. 105, pp. 188-210, May 2018.

[3] M. A. Agnero, K. Konan, Z. G. C. S. Tokou, Y. T. A. Kossonou, B. S. Dion, K. A. Kaduki, et al., "Malaria-Infected Red Blood Cell Analysis through Optical and Biochemical Parameters Using the Transport of Intensity Equation and the Microscope's Optical Properties," Sensors, vol. 19, no. 14, article no. 3045, July 2019.

[4] K. Torres, C. M. Bachman, C. B. Delahunt, J. A. Baldeon, F. Alava, D. G. Vilela, et al., "Automated Microscopy for Routine Malaria Diagnosis: A Field Comparison on Giemsa-Stained Blood Films in Peru," Malaria Journal, vol. 17, article no. 339, 2018.

[5] C. T. Kozycki, N. Umulisa, S. Rulisa, E. I. Mwikarago, J. P. Musabyimana, J. P. Habimana, et al., "False-Negative Malaria Rapid Diagnostic Tests in Rwanda: Impact of Plasmodium falciparum Isolates Lacking Hrp2 and Declining Malaria Transmission," Malaria Journal, vol. 16, article no. 123, 2017.

[6] Z. A. Abdalla, N. E. A. Rahma, E. E. Hassan, T. M. Abdallah, H. E. Hamad, S. A. Omer, et al., "The Diagnostic Performance of Rapid Diagnostic Tests and Microscopy for Malaria Diagnosis in Eastern Sudan Using a Nested Polymerase Chain Reaction Assay as a Reference Standard," Transactions of the Royal Society of Tropical Medicine and Hygiene, vol. 113, no. 11, pp. 701-705, November 2019.

[7] S. L. R. Yan, F. Wakasuqui, and C. Wrenger, "Point-of-Care Tests for Malaria: Speeding Up the Diagnostics at the Bedside and Challenges in Malaria Cases Detection," Diagnostic Microbiology and Infectious Disease, vol. 98, no. 3, article no. 115122, November 2020.

[8] K. O. Mfuh, S. T. Yunga, L. F. Esemu, O. N. Bekindaka, J. Yonga, J. C. Djontu, et al., "Detection of Plasmodium falciparum DNA in Saliva Samples Stored at Room Temperature: Potential for a Non-Invasive Saliva-Based Diagnostic Test for Malaria," Malaria Journal, vol. 16, article no. 434, 2017.

[9] G. V. Soraya, C. D. Abeyrathne, C. Buffet, D. H. Huynh, S. M. Uddin, J. Chan, et al., "Ultrasensitive and Label-Free Biosensor for the Detection of Plasmodium falciparum Histidine-Rich Protein II in Saliva," Scientific Reports, vol. 9, article no. 17495, 2019.

[10] O. Rifaie-Graham, J. Pollard, S. Raccio, S. Balog, S. Rusch, M. A. Hernández-Castañeda, et al., "Hemozoin-Catalyzed Precipitation Polymerization as an Assay for Malaria Diagnosis," Nature Communications, vol. 10, article no. 1369, 2019.

[11] W. A. Oyibo, N. Ezeigwe, G. Ntadom, O. O. Oladosu, K. Rainwater-Loveth, W. O'Meara, et al., "Multicenter Pivotal Clinical Trial of Urine Malaria Test for Rapid Diagnosis of Plasmodium falciparum Malaria," Journal of Clinical Microbiology, vol. 55, no. 1, pp. 253-263, January 2017.

[12] F. Maurin, C. Claeys, E. Deckers, and W. Desmet, "Probability that a Band-Gap Extremum is Located on the Irreducible Brillouin-Zone Contour for the 17 Different Plane Crystallographic Lattices," International Journal of Solids and Structures, vol. 135, pp. 26-36, March 2018.

[13] H. A. Elsayed, F. A. Sayed, and A. H. Aly, "Graphene Deposited Liquid Crystal and Thermal Sensitivity Using Photonic Crystals," Physica Scripta, vol. 96, no. 3, article no. 035503, March 2021.

[14] S. Dinodiya and A. Bhargava, "A Comparative Analysis of Pressure Sensing Parameters for Two Dimensional Photonic Crystal Sensors Based on Si and GaAs," Silicon, vol. 14, no. 9, pp. 4611-4618, June 2022.

[15] Z. A. Zaky, A. M. Ahmed, A. S. Shalaby, and A. H. Aly, "Refractive Index Gas Sensor Based on the Tamm State in a One-Dimensional Photonic Crystal: Theoretical Optimisation," Scientific Reports, vol. 10, article no. 9736, 2020.

[16] S. Agarwal, J. K. Mishra, and V. Priye, "Highly Sensitive MOEMS Integrated Photonic Crystal Cavity Resonator for Nano-Mechanical Sensing," Optics Communications, vol. 474, article no. 126150, November 2020.

[17] J. N. Ansari, S. C. Gowre, M. V. Sonth, B. Gadgay, and A. S. Roy, "Photonic Nano Dielectric Crystal Cavity with Infiltrated Biosamples for Refractive Index Sensing Application," Integrated Ferroelectrics, vol. 213, no. 1, pp. 93-102, 2021.

[18] Ankita, S. Bissa, B. Suthar, C. Nayak, and A. Bhargava, "An Improved Optical Biosensor Design Using Defect/Metal Multilayer Photonic Crystal for Malaria Diagnosis," Results in Optics, vol. 9, article no. 100304, December 2022.

[19] B. M. H. Kumar, P. C. Srikanth, and A. M. Vaibhav, "A Novel Computation Method for Detection of Malaria in RBC Using Photonic Biosensor," International Journal of Information Technology, vol. 13, no. 5, pp. 2053-2058, October 2021.

[20] A. Rashidnia, H. Pakarzadeh, M. Hatami, and N. Ayyanar, "Photonic Crystal-Based Biosensor for Detection of Human Red Blood Cells Parasitized by Plasmodium falciparum," Optical and Quantum Electronics, vol. 54, no. 1, article no. 38, January 2021.

[21] H. Tayoub, A. Hocini, and A. Harhouz, "Malaria Diagnosis Using High Quality-Factor Photonic Crystal Biosensor," 21st International Conference on Numerical Simulation of Optoelectronic Devices, article no. P13pd, September 2021.

[22] N. A. Mohammed, M. M. Hamed, A. A. M. Khalaf, and S. El-Rabaie, "Malaria Biosensors with Ultra-Sensitivity and Quality Factor Based on Cavity Photonic Crystal Designs," The European Physical Journal Plus, vol. 135, no. 11, article no. 933, November 2020.

[23] Ankita, B. Suthar, and A. Bhargava, "Biosensor Application of One-Dimensional Photonic Crystal for Malaria Diagnosis," Plasmonics, vol. 16, no. 1, pp. 59-63, February 2021.

[24] S. K. Saini and S. K. Awasthi, "Sensing and Detection Capabilities of One-Dimensional Defective Photonic Crystal Suitable for Malaria Infection Diagnosis from Preliminary to Advanced Stage: Theoretical Study," Crystals, vol. 13, no. 1, article no. 128, January 2023.

[25] M. N, S. Raga, S. K. Gowre, H. Miyan, and P. Sharan, "Two-Dimensional Photonic Crystal Biosensor Based on Gallium Arsenide Composite Semi-conductive Material for Diabetes Detection," Plasmonics, vol. 18, pp. 1429-1440, May 2023.

[26] H. Miyan, R. Agrahari, S. K. Gowre, M. Mahto, and P. K. Jain, "Computational Study of a Compact and High Sensitive Photonic Crystal for Cancer Cells Detection," IEEE Sensors Journal, vol. 22, no. 4, pp. 3298-3305, February 2022.
[27] L. S. Puumala, S. M. Grist, K. Wickremasinghe, M. A. Al-Qadasi, S. J. Chowdhury, Y. Liu, et al., "An Optimization Framework for Silicon Photonic Evanescent-Field Biosensors Using Sub-Wavelength Gratings," Biosensors, vol. 12, no. 10, article no. 840, October 2022.
[28] H. Miyan, R. Agrahari, S. K. Gowre, P. K. Jain, and M. Mahto, "Computational Study of 2D Photonic Crystal Based Biosensor for SARS-COV-2 Detection," Measurement Science and Technology, vol. 34, no. 7, article no. 074004, July 2023.
[29] M. G. Daher, "Supersensitive Biosensor Based on a Photonic Crystal Nanostructure for Blood Sugar Level Monitoring with Ultra-High Quality Factor and Low Detection Limit," Optik, vol. 275, article no. 170581, March 2023.